Improved initial discharge capacity of nanostructured Ni-Co spinel ferrite as anode material in lithium ion batteries

CrossMark

Emad M. Masoud *

Chemistry Department, Faculty of Science, Benha University, 13518 Benha, Egypt

ARTICLE INFO

ABSTRACT

Nanostructured nickel ferrite doped with cobalt is synthesized by co-precipitation method. The sample is characterized using X-ray diffraction, Fourier Transform Infra Red and Transmission Electron Microscope. Specific surface area and porosity analysis are performed through Brunauer–Emmett–Teller (BET) nitrogen adsorption–desorption isotherms. The magnetic properties are also studied. Spinel cubic structure with nanoparticles and porous surface is confirmed. The electrochemical properties of the nanostructured spinel are investigated including the cycling performance as anode material for lithium ion batteries. The results show that the sample has a high discharge capacity, especially the first five cycles, at current density of 2.43 mA/cm^2 compared to recent performances reported at low current density (0.2 mA/cm^2) for pure and composite of nanonickel ferrite. All results and data are correlated and discussed.

1. Introduction

Owing to the high operating voltage, high energy density, low self discharge rate and long service life, rechargeable lithium-ion batteries (LIBS) are extremely promising power sources for various electronic devices [1–5]. However, the performance of rechargeable LIBS strongly depends on electrode materials, and the hunt for nanostructured high performance LIBs electrode materials remains the main research objectives [6–10]. Recently, nanostructured Fe-based ferrites with higher specific capacities have been explored as anode material in LIBs. Unfortunately, the batteries using such materials display low discharge capacity especially at high current density. As a number of Fe-based ferrites, $NiFe_2O_4$ have displayed a good electrochemical behavior and a high theoretical capacity (914 mAh/g) [11]. The high discharge capacity and cycle life at high current density are still the important and basic goal for these electrodes working in lithium batteries. The metal doping of such nanonickel ferrites structures is still not used enough to improve the electrochemical properties of nickel ferrite, especially the high discharge capacity value and cycle life stability at high current density. In this work, we try to use Co-doped nanonickel ferrite to retain a high discharge capacity value with good cycle life at high current density.

2. Experimental

2.1. Synthesis

Nickel, cobalt and iron nitrate were taken in a 0.5: 0.5:2 mole ratio (molarity of Fe^{3+} is doubled that of divalent cations) and dissolved in deionized water. This mixture was co-precipitated with urea at 90 °C under constant stirring. The precipitate was filtered and washed several times with deionized water to get rid of the nitrates; finally the mixture was dried in an oven overnight at 120 °C. The precursor was calcined at 600 °C for 4 h.

2.2. Characterization

X-ray diffraction analysis was performed on a Diano (made by Diano Corporation, U.S.A.). The pattern was run with Cu-filtered CuKα radiation ($\lambda = 1.5418$ Å) energized at 45 kV, and 10 mA. The sample was measured at room temperature in the range from $2\theta = 10$ to 80°. The XRD planes present in the sample were identified with the help of ASTM Powder Data Files. The infrared spectra of the sample were recorded in the range of 350–3850 cm^{-1} using a Brucker-FTIR. The morphology of sample was examined using transmission electron microscope (TEM, JEOL-2010) operated at an accelerating voltage of 200 kV. Specific surface area and porosity analysis for the sample was performed through measuring Brunauer–Emmett–Teller (BET) nitrogen adsorption–desorption isotherm with a Micromeritics ASAP2020 apparatus. The magnetic measurement was carried out at room temperature by a VSM (Vibrating Sample Magnetometer, BHV-55) technique.

2.3. Electrochemical measurements

To set up the experimental cell, $Ni_{0.5}Co_{0.5}Fe_2O_4$ powder (75 wt.%, 21.25 mg/cm^2) was mixed with carbon black (10 wt.%), graphite (10 wt.%) and PVDF (5 wt.%) in the presence of n-methylpyrrolidinone to make the mixture homogeneous and then the mixture was left on a hot plate for 3 h. to evaporate the homogeneity material. After that, a

* Corresponding author. Tel.: 002-01203532343.
E-mail address: emad_masoud1981@yahoo.com.
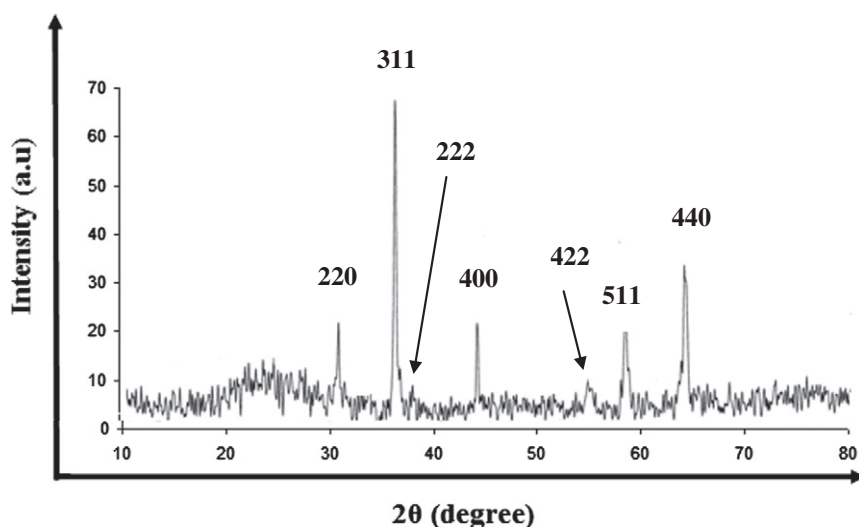
Fig. 1. XRD pattern of nano$Ni_{0.5}Co_{0.5}Fe_2O_4$.
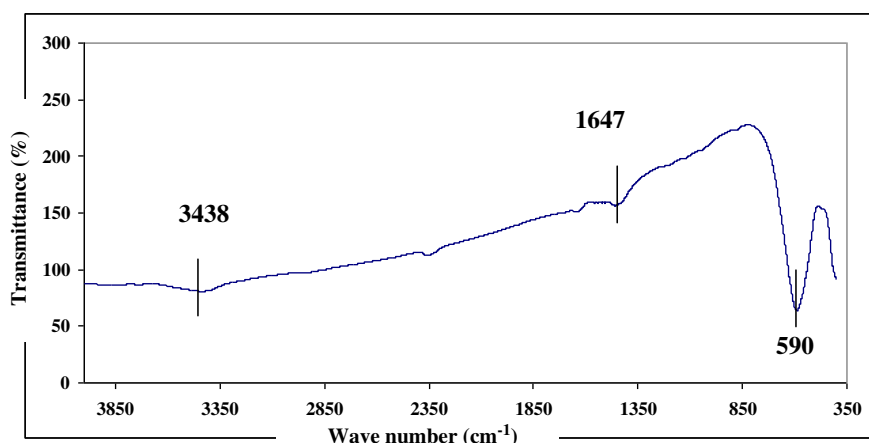
Fig. 2. FTIR spectrum of nano $Ni_{0.5}Co_{0.5}Fe_2O_4$.

certain weight of the powder was coated onto cupper foil and some drops of n-methylpyrrolidinone were added again and then the powder was dried under vacuum for 30 min at 120 °C. In a glove box under argon atmosphere, the cell was constructed as coin-type cells. A porous polypropylene film was used for separating the cathode and a lithium metal anode, and a mixture of 1 M $LiPF_6$-ethylene carbonate/dimethyl carbonate (1:1, v/v, Merck) was used as the electrolyte. The cell was galvanostatically charged and discharged using EG&G Electrochemical analyzer (Model-6310) in the scan rate of 1 mV/s to perform charge–discharge processes for the assembled battery. The charge–discharge processes were performed at a voltage between 0.1 and 3 V and a current density of 2.43 mA/cm², the current density was calculated by dividing the applied current of 1 C by the surface area of the used coated Cu-foil.

3. Results and discussion

Fig. 1 shows the room-temperature XRD pattern of as-prepared $Ni_{0.5}Co_{0.5}Fe_2O_4$. The presence of lattice planes, (220), (311), (222), (400), (422), (511) and (440), which indexed to nickel ferrite [12] confirms the formation of spinel cubic structure (JCPDS file No. 86-2267, Fd-3 m). No peaks of impurities can be observed, confirming the purity of sample. The particle size was calculated using Scherrer's formula, $D = 0.89\,\lambda\,/\,\beta\,\cos\,\theta$ [13], where D is the crystallite size, 0.89

is the Scherrer constant, λ is the X-ray wavelength, β is the full-width at half of peak and θ is the corresponding Bragg angle. The calculated average crystallite size was found to equal to 76 nm.

FTIR bands of solid are generally assigned to clarify vibration of ions of tetrahedral and octahedral complexes of spinel structures [14]. Fig. 2 shows the FTIR spectrum of the powder. Three sharp characteristic
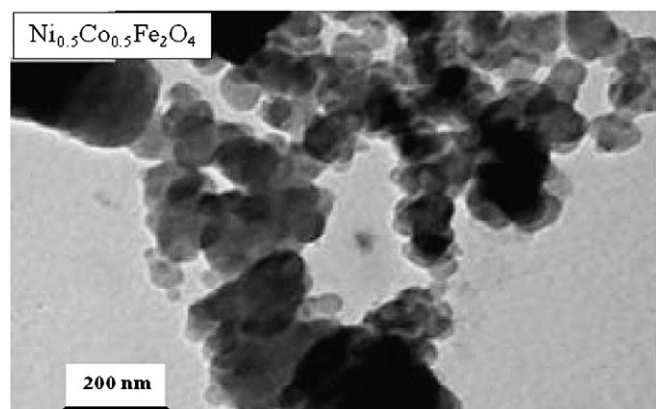
Fig. 3. TEM of nano$Ni_{0.5}Co_{0.5}Fe_2O_4$.
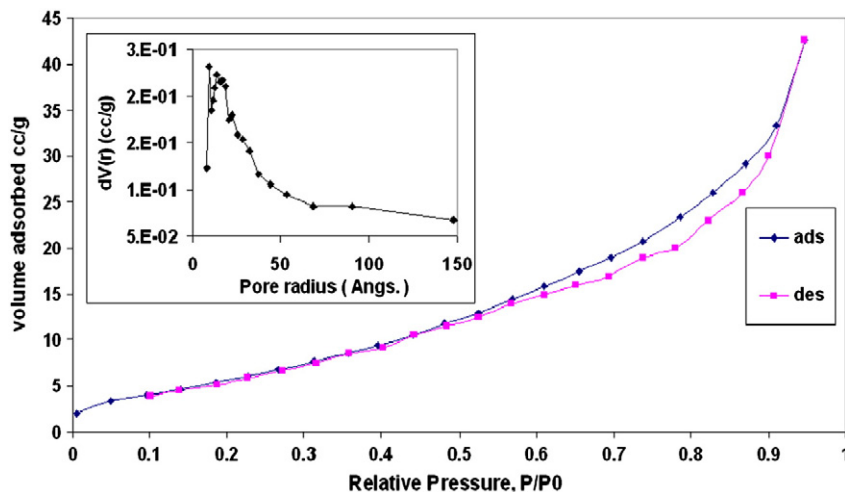
Fig. 4. N_2 adsorption/desorption isotherm curve of nanoNi$_{0.5}$Co$_{0.5}$Fe$_2$O$_4$ and Barrett–Joyner–Halenda (BJH) pore size distribution plot (inset).

absorption bands can be clearly seen. The bands at 3438 and 1647 cm^{-1} are assigned to the OH vibrations of the adsorbed H_2O [14]. The absorption band at 590 cm^{-1} corresponds to stretching vibration of tetrahedral groups Fe–O [14]. Also, this absorption band is a characteristic of inverse spinel ferrites [15,16].

Fig. 3 shows TEM image of Ni$_{0.5}$Co$_{0.5}$Fe$_2$O$_4$. The image showed aggregated nanosphere particles with porous structure produced by

the assembly of small particles among the agglomerated. The aggregation of these particles is caused by the intrinsic magnetic characteristic of NiFe$_2$O$_4$.

Usually, spherical shapes are formed because the nucleation rate per unit area is isotopic at the interface between the Ni–Co ferrite magnetic nanoparticles, which is the driving force for Ostwald ripening. This produces a minimization in the surface free energy by reduction of
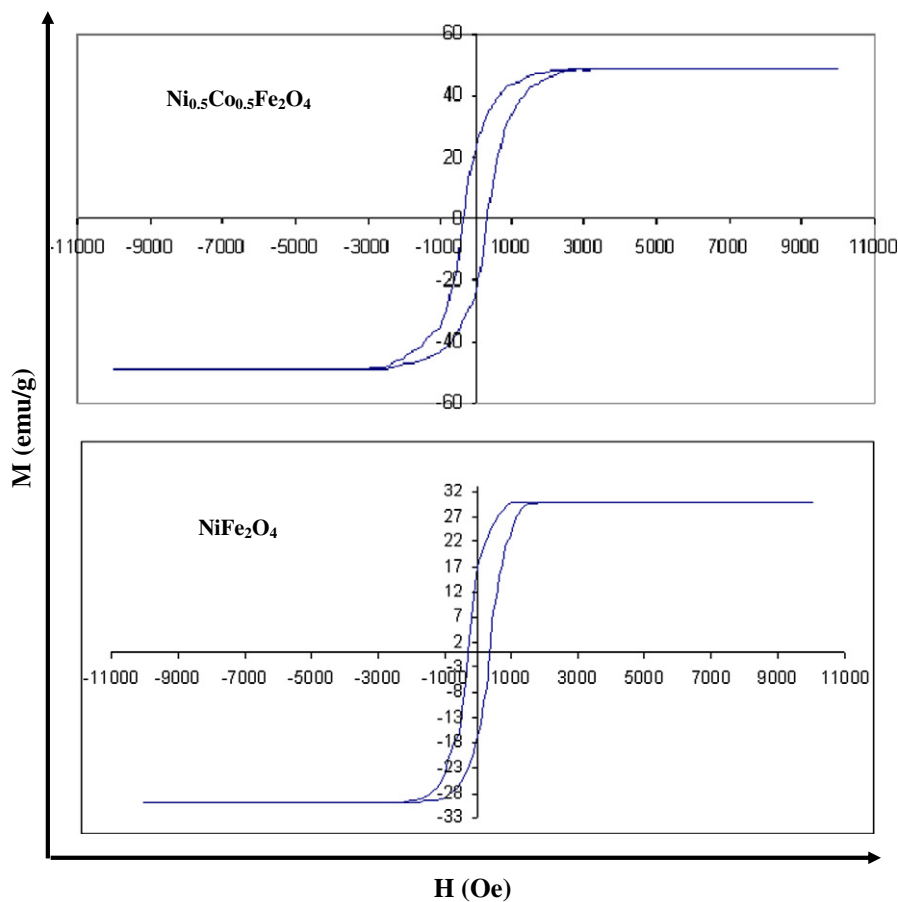
Fig. 5. Magnetic hysteresis loops of nanoNiFe$_2$O$_4$ and Ni$_{0.5}$Co$_{0.5}$Fe$_2$O$_4$ samples.

Table 1
Comparison of the electrochemical properties of nano$Ni_{0.5}Co_{0.5}Fe_2O_4$.

Sample	Particle size (nm)	Current density (mA/cm^2, C)	Potential range (V)	Initial capacity (mAh/g)	Capacity retention (mAh/g)	References
$Ni_{0.5}Co_{0.5}Fe_2O_4$	76 nm	2.43	0.1–3	1100	720 after five cycles	This work
$NiFe_2O_4$	21–125 nm	0.2	0–3	1400	830 after five cycles	[12]
$NiFe_2O_4$	5–15 nm	0.2	0–3	1314	709 after three cycles	[18]
$NiFe_2O_4$/C	50–100 nm	1/8 C	0.01–3	1250	810 after five cycles	[11]

Table 2
Values of lattice parameter a and X-ray density for nano $NiFe_2O_4$ and $Ni_{0.5}Co_{0.5}Fe_2O_4$ samples.

Sample	a (Å)	density (g/cm^3)
$NiFe_2O_4$	8.334	5.4
$Ni_{0.5}Co_{0.5}Fe_2O_4$	8.366	5.3

Table 3
Values of saturated magnetization (Ms, emu) and coercivity (Hc, Oe) for nano $NiFe_2O_4$ and $Ni_{0.5}Co_{0.5}Fe_2O_4$ samples.

Sample	M_s (emu)	H_c (Oe)
$NiFe_2O_4$	29.7	325
$Ni_{0.5}Co_{0.5}Fe_2O_4$	48.8	340

total surface area/volume, which results in the equivalent growth rate along different directions of the nucleation because the sphere has the smallest surface area per unit volume of any shape.

The textural properties of nano$Ni_{0.5}Co_{0.5}Fe_2O_4$ were further investigated by nitrogen sorption and desorption isotherms and corresponding pore size distribution (inset) is shown in Fig. 4. It can be seen that the specific surface area is calculated using BET method and is determined to be 25 m^2/g. The pore size distribution reveals a mean pore radius of 9.37 Å. Also, the pore volume was determined to be 0.182 cc/g.

The magnetic properties of nano$Ni_{0.5}Co_{0.5}Fe_2O_4$ were also characterized and compared to a pure nickel ferrite ($NiFe_2O_4$) sample prepared with the same method (Fig. 5) to show the effect of Ni substitution by cobalt during the conversion reaction in the electrochemical characterization. Fig. 5 showed that Co-doping enhanced both values of saturated magnetization (M_s) and coercivity (H_c) compared to the undoped sample. The values of M_s and H_c are listed in Table 3.

The enhancement of magnetic parameters can be attributed to the high magnetic moment of cobalt compared to nickel. This enhancement may play a role in enhancing the electrical contact and keep integrity during the conversion reaction of the electrochemical cell as will be seen later.

Fig. 6 shows typical charge–discharge curve at 2.43 mA/cm^2 current density. The initial discharge curve shows a clear potential plateau at around 0.6 V. This plateau corresponds to the following proposed reaction [17]:

$$Ni_{0.5}Co_{0.5}Fe_2O_4 + 8Li^+ + 8e^- \rightarrow 0.5Ni + 0.5Co + 2Fe + 4Li_2O. \quad (1)$$

The slopping part at the end of the discharge curve (between 0.6 and 0 V) corresponds to the formation of the solid electrolyte interface.

Also, there is a one slop around 1.6 V in each charge curve which corresponds to the following charge reaction:

$$0.5Ni + 0.5Co + 2Fe + 4Li_2O \rightarrow Ni_{0.5}Co_{0.5}Fe_2O_4 + 8Li^+ + 8e^-. \quad (2)$$

It is observed from literature [12] that the value of $NiFe_2O_4$ cathodic reaction voltage is shifted due to cobalt doping or/and particle size from 0.4 to 0.6 V.

In order to investigate the lithium storage capacities of porous $Ni_{0.5}Co_{0.5}Fe_2O_4$ nanospheres, galvanostatic charge/discharge cycling at a current density of 2.43 mA/cm^2 was determined (Fig. 7). The figure showed that the first charge and discharge capacities of nano$Ni_{0.5}Co_{0.5}Fe_2O_4$ have high values of 820 mAh/g and 1100 mAh/g, respectively. The capacity retention through the first five cycles is good as the value of capacity for charge and discharge is 700 mAh/g and 718 mAh/g for the fifth cycle, respectively. This sample has a good performance through the first five cycles compared to the previous reported performances of pure and composite of nickel ferrite such as $NiFe_2O_4$ nanospheres [12], $NiFe_2O_4$ nanoquadrate [18] and nano$NiFe_2O_4$/C [11] that showed a good discharge capacity at low current density (0.2 mA/cm^2, 0.2 mA/cm^2 and 1/8 C, respectively),
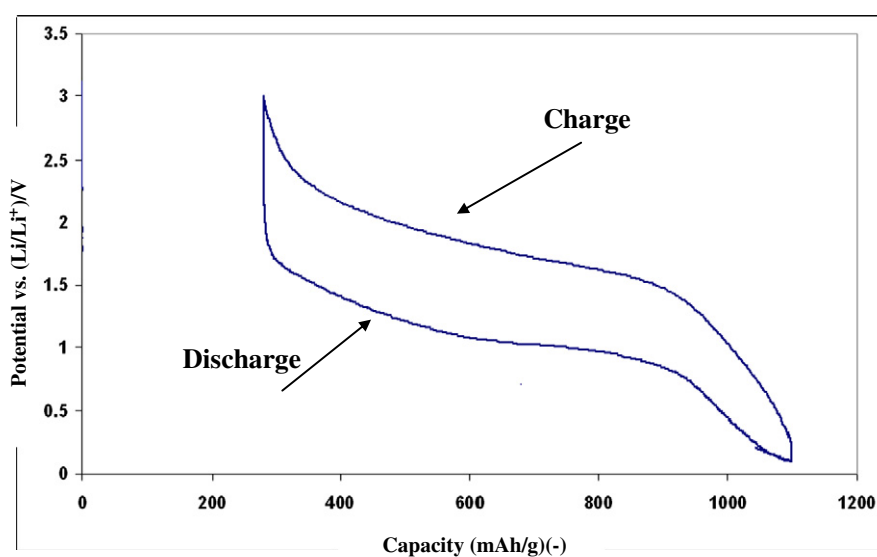
Fig. 6. Galvanostatic lithium insertion/extraction curve of $Ni_{0.5}Co_{0.5}Fe_2O_4$ electrode between 0.1 and 3 V at a current density of 2.43 mA/cm^2.
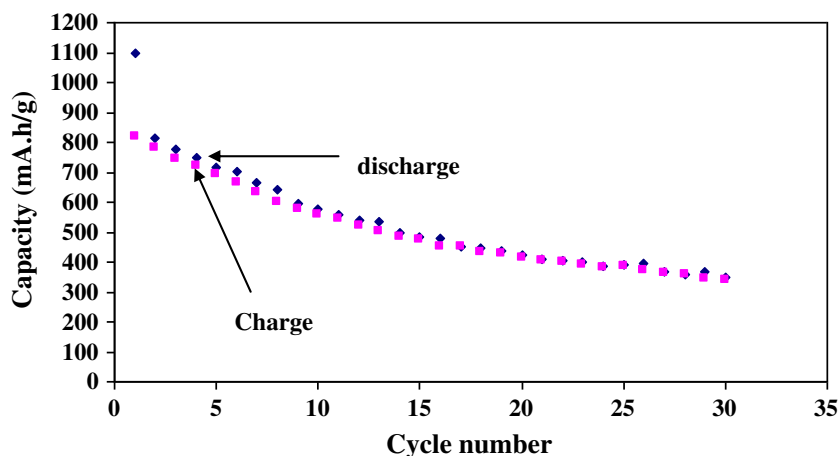
Fig. 7. Charge–discharge capacity against cycle number for nanoNi$_{0.5}$Co$_{0.5}$Fe$_2$O$_4$ sample at a current density of 2.43 mA/cm^2.

respectively, Table 1. A comparison of the electrochemical properties of nanoNi$_{0.5}$Co$_{0.5}$Fe$_2$O$_4$ with the recent studies is shown in Table 1. Several factors such as surface area, particle size, and structure stability are competing with each other, which may affect the Li-ion storage performance [19–21]. Also, in the previous reports, Zhu et al. summarized that the optimal grain size, crystallinity and morphology codetermined the property of anode material [20]. Yan et al. also reached a similar conclusion and further pointed out that well-crystalline material could maintain the nanocrystallite size and activate the decomposition of Li$_2$O, thus increasing the discharge capacity [19]. Also, as we all know, the diffusion length for lithium ion and electron is especially important for cycling [22]. The small particle size can reduce the mean Li diffusion pathways and increase the contact surface area between the anode and the electrolyte [23]. These effects can promote faster ionic transport and contribute to faster charge–discharge processes in secondary lithium batteries [24]. Also, it is well known that a large surface area is important for the improvement of reaction performance, in terms of the introduction of lithium ions through the nickel oxide surface. The capacity and affinity will be greatly enhanced when the surface area is high, since the diffusion lengths of the lithium ions are greatly shortened [25]. Therefore, the materials with small particle size and high surface area would exhibit the highest discharge capacity [26].

Moreover, the porous structure with large surface to volume ratio and short diffusion length for lithium intercalation can lead to superior cycling and rate performance of electrode materials [27,28]. For our investigated sample, the pore structure confirmed by TEM provides a space for volume expansion during lithiation. Moreover, these grains enlarge and adhere together to form a compact layer, which have high stability and preserve the integrity of the structure.

Also, the porous structure can not only benefit the diffusion of solid state Li-ion [21,29–32], but also accommodate volume changes of charge/discharge process to maintain the structure integrity [33,34].

In addition to what was mentioned above, the doping process using cobalt can cause an expansion of the lattice crystal confirmed by increasing the values of lattice parameter a and X-ray density for doped ferrite compared to the pure one (Table 2). This expansion could provide more lattice space for lithium intercalation/deintercalation and enhance the diffusion of lithium ion, and further improves the reversible capacities and cycling performance of Ni$_{0.5}$Co$_{0.5}$Fe$_2$O$_4$ [35].

At the same time, the efficiency behavior of nanoNi$_{0.5}$Co$_{0.5}$Fe$_2$O$_4$ through charge–discharge processes confirmed that the sample has a good efficiency (Fig. 8). It shows that the efficiency of the first and last cycles was 74.5% and 97%, respectively. The extradischarge capacities are mainly due to the decomposition of non-aqueous electrolyte during the discharge process [36].

4. Conclusions

Ni–Co spinel ferrite was prepared using co-precipitation method. The sample was characterized using different techniques like X-ray diffraction, FTIR, TEM and nitrogen adsorption/desorption isotherms.
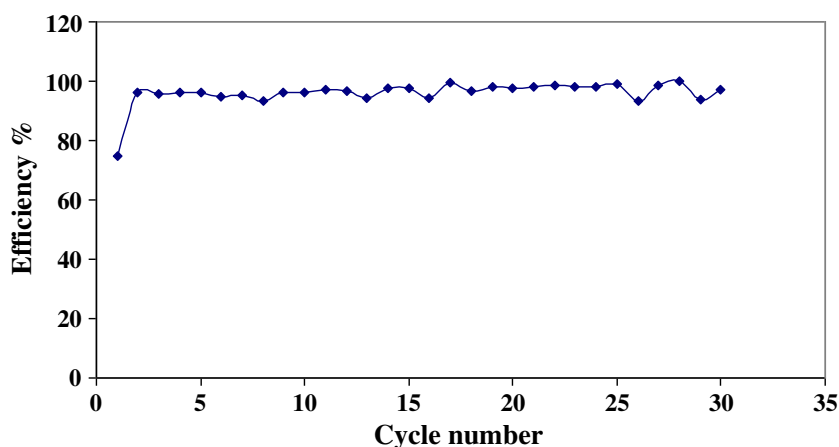
Fig. 8. Cycle number dependence of efficiency for nanoNi$_{0.5}$Co$_{0.5}$Fe$_2$O$_4$ sample.

Characterization techniques showed that $Ni_{0.5}Co_{0.5}Fe_2O_4$ has pure spinel cubic structure with particle size equal to 76 nm and nanosphere shape with porous structure. Electrochemical tests at current density of 2.43 mA/cm^2 showed that the sample has a good discharge capacity, especially for the first five cycles, compared to recent previous studies. The sample delivered initial discharge and charge capacities of 1100 and 820 mAhg^{-1}, respectively. The improved electrochemical behavior at 2.43 mA/cm^2 compared to recent studies at low current density can be attributed to the doping effect, nanoparticle size, and porous structure.

Acknowledgments

References

[1] S. Zugmann, D. Moosbauer, M. Amereller, C. Schreiner, F. Wudy, R. Schmitz, R. Schmitz, P. Isken, C. Dippel, R. Müller, M. Kunze, A. Lex-Balducci, M. Winter, H.J. Gores, J. Power Sources 196 (2011) 1417.
[2] G. Zhou, D.W. Wang, F. Li, L. Zhang, N. Li, Z.S. Wu, L. Wen, G.Q. Lu, H.M. Cheng, Chem. Mater. 22 (2010) 5306.
[3] Y.H. Xu, Rare Met. Mater. Eng. 32 (2003) 875.
[4] J.B. Goodenough, Y. Kim, Chem. Mater. 22 (2010) 587.
[5] J.B. Goodenough, Y. Kim, Chem. Mater. 22 (2009) 587.
[6] Y. Zou, Y. Wang, ACS Nano 5 (2011) 8108.
[7] X. Zhu, Y. Zhu, S. Murali, M.D. Stoller, R.S. Ruoff, ACS Nano 5 (2011) 3333.
[8] S. Yoon, A. Manthiram, Electrochim. Acta 56 (2011) 3029.
[9] Z.G. Yang, D. Choi, S. Kerisit, K.M. Rosso, D.H. Wang, J. Zhang, G. Graff, J. Liu, J. Power Sources 192 (2009) 588.
[10] J.R. Szczech, S. Jin, Energy Environ. Sci. 4 (2011) 56.
[11] Yu Ding, Yifu Yang, Huixia Shao, power sources 244 (2013) 610–613.
[12] H. Liu, H. Zhu, H. Yang, Mater. Res. Bull. 48 (2013) 1587.
[13] W.E. Mahmoud, H. El-Mallah, J. Phys. D. Appl. Phys. 42 (2009) 035502.
[14] M. Srivastava, A.K. Ojha, S. Chaubey, A. Materny, J. Alloys Compd. 481 (2009) 515.
[15] M. Gotic, I. Czako–Nagy, S. Popovic, S. Music, Philos. Magn. Lett. 78 (1998) 193.
[16] J.L. Gunjakar, A.M. More, V.R. Shinde, C.D. Lokhande, J. Alloys Compd. 465 (2008) 468.
[17] X.H. Huang, J.P. Tu, B. Zhang, C.Q. Zhang, Y. Li, Y.F. Yuan, H.M. Wu, J. Power Sources 161 (2006) 541.
[18] H. Zhao, Z. Zheng, K.W. Wong, S. Wang, B. Huang, D. Li, Electrochem. Commun. 9 (2007) 2606.
[19] N. Yan, L. Hu, Y. Li, Y. Wang, H. Zhong, X.Y. Hu, X.K. Kong, Q.W. Chen, J. Phys. Chem. C 116 (2012) 7227.
[20] J.X. Zhu, Y.K. Sharma, Z.Y. Zeng, X.J. Zhang, M. Srinivasan, S. Mhaisalkar, H. Zhang, H.H. Hng, Q.Y. Yan, J. Phys. Chem. C 115 (2011) 8400.
[21] X.W. Lou, D. Deng, J.Y. Lee, L.A. Archer, J. Mater. Chem. 18 (2008) 4397.
[22] G. Zhang, Y. Chen, B. Qu, L. Hu, L. Mei, D. Lei, Q. Li, L. Chen, Q. Li, T. Wang, Electrochim. Acta 80 (2012) 140.
[23] S.H. Choi, J.W. Son, Y.S. Yoon, J. Kim, Power Sources 158 (2006) 1419.
[24] J.M. Tarascon, M. Armand, Nature 414 (2001) 359(456).
[25] Y. Nuli, R. Zeng, P. Zhang, Z. Guo, H. Liu, Power Sources 184 (2008).
[26] S.Y. Zeng, K.B. Tang, T.W. Li, J. Colloid Interface Sci. 312 (2007) 513.
[27] B.H. Qu, M. Zhang, D.L. Lei, Y.P. Zeng, Y.J. Chen, L.B. Chen, Q.H. Li, Y.G. Wang, T.H. Wang, Nanoscale 3 (2011) 3646.
[28] J.T. Zai, X.F. Qian, K.X. Wang, C. Yu, L.Q. Tao, Y.L. Xiao, J.S. Chen, CrystEngComm 14 (2012) 1364.
[29] B.Q. Liu, Q.F. Li, B. Zhang, Y.L. Cui, H.F. Chen, G.N. Chen, D.P. Tang, Nanoscale 3 (2011) 2220.
[30] D.W. Liu, B.B. Garcia, Q.F. Zhang, Q. Guo, Y.H. Zhang, S. Sepehri, G.Z. Cao, Adv. Funct. Mater. 19 (2009) 1015.
[31] C.M. Park, J.K. Jeon, Chem. Commun. 47 (2011) 2122.
[32] H.S. Zhou, D.L. Li, M. Hibino, I. Honma, Angew. Chem. Int. Ed. 44 (2005) 797.
[33] S.M. Yuan, J.X. Li, L.T. Yang, L.W. Su, L. Liu, Z. Zhou, Appl. Mater. Interfaces 3 (2011) 705.
[34] C. Burda, X.B. Chen, R. Narayanan, M.A. El-sayed, Chem. Rev. 105 (2005) 1025.
[35] Q. Wang, Y. Huang, J. Miao, Y. Zhao, Y. Wang, Electrochim. Acta 93 (2013) 120.
[36] S. Grugeon, S. Laruelle, R. Herrera–Urbina, L. Dupont, P. Poizot, J.M. Tarascon, J. Electrochem. Soc. 148 (2001) A285.